



Impact of PEDOT: PSS Electrode Work Function on DPPEZnP-TBO Based Active Layer in Tandem Organic Solar Cells

SANJAY NARAYAN BARMAN and PINAKI LAHA*

Department of Physics, B.R. Ambedkar Bihar University, Muzaffarpur.

Abstract

This study investigates the impact of electrode work function on the performance and efficiency of DPPEZnP-TBO-based tandem organic solar cell (OSC) devices, focusing on PEDOT: PSS as the electrode material. By adjusting the electrode's work function, we investigate its influence on the active layer's electrical properties and the device's key performance metrics, including open-circuit voltage (V_{oc}), short-circuit current density (J_{sc}), power conversion efficiency (PCE), and fill factor (FF). Changes in electrode work function are associated with significant differences in fill factor (FF), power conversion efficiency (PCE), open-circuit voltage (V_{oc}), and short-circuit current density (J_{sc}). The best performance is of tandem organic solar cell is achieved at a work function of 5.2 eV, with a J_{sc} of 2.598 mA/cm², V_{oc} of 1.16 V, PCE of 2.41%, and FF of 79.6%. Optimising the work function improves charge mobility and reduces recombination losses, enhancing overall performance. This research provides valuable insights into improving DPPEZnP-TBO solar cells for durable and scalable large-scale solar energy applications.



Article History

Received: 09 December 2025

Accepted: 26 December 2025

Keywords

DPPEZnP-TBO;
Fill Factor (FF);
Organic Tandem Solar Cells ;
Power Conversion Efficiency (PCE);
Work Function.

Introduction

Population growth and the post-COVID industrial resurgence have led to a significant increase in energy demand.¹⁻⁴ Researchers have suggested a variety of renewable energy sources to lessen reliance on fossil fuels, with solar energy emerging as the most favoured choice.² In recent decades, organic photovoltaic technology has garnered growing interest. Organic solar cells (OSCs) serve as a cost-efficient substitute for standard inorganic

solar cells.^{1,2} OSCs' demand lies in their versatility, flexibility, lightweight design, and affordability.³⁻⁶ To produce low-cost organic solar cells, it is highly desirable to eliminate metal electrodes and indium-tin-oxide (ITO), due to the high cost of ITO and its limited mechanical flexibility.^{4, 7} Additionally, the deposition of metal electrodes requires high-vacuum environments, which are not conducive to cost-effective and large-scale production. Research on electrode work function is crucial as it governs

CONTACT Pinaki Laha ✉ lahapi007@gmail.com 📍 Department of Physics, B.R. Ambedkar Bihar University, Muzaffarpur.



© 2025 The Author(s). Published by Enviro Research Publishers.

This is an Open Access article licensed under a Creative Commons license: Attribution 4.0 International (CC-BY).

Doi: <http://dx.doi.org/10.13005/msri/220303>

charge extraction through proper energy level alignment between electrodes and active layers.⁸ Proper alignment minimises interfacial barriers and enhances carrier collection in tandem cells. Organic solar cell devices are more stable and efficient when their work functions are optimised. Comparative summary of solar cell devices employing ITO/PEDOT: PSS-based electrodes, highlighting their fill factors and power conversion efficiencies in Table 1.⁹⁻¹³ Due to their superior transparency, high conductivity (above 1000 S/cm), and compatibility with solution-based processing methods like spin coating, spraying, and printing, conductive polymers, such as poly(3,4-ethylenedioxythiophene)-poly(styrene sulfonate) (PEDOT: PSS), have emerged as promising substitutes for ITO for bottom electrodes. PEDOT: PSS has also been utilised as a top electrode in organic solar cells with inverted structures.¹⁴⁻¹⁶ PEDOT: PSS is appropriate for hole collection in organic solar cells since it usually shows a working function of about 5.0 eV.¹⁷ Nevertheless, it is still difficult to obtain a low work function (LWF) PEDOT: PSS for electron collecting.^{18,19} In earlier methods, a ZnO layer was deposited on PEDOT: PSS to help with electron collection. According to recent research, organic compounds such as polyethylenimine (PEI) and polyethylenimine ethoxylated (PEIE) can successfully reduce the work function of different conductors, such as PEDOT: PSS. Researchers have created ITO- and

metal-electrode-free organic solar cells utilising LWF-PEDOT: PSS, however, the device efficiencies have remained comparatively low, at about 3%.²⁰ The low fill factor (around 52%) resulting from PEDOT: PSS restricted conductivity is the main cause of this low efficiency value. According to recent research, sulphuric acid post-treatment can significantly raise PEDOT: PSS conductivity to over 2000 S/cm.¹⁷ This improvement has the potential to increase the efficiency of organic photovoltaic cells that use PEDOT: PSS as the top and bottom electrodes. Furthermore, although spin coating has historically been used to apply PEI and PEIE modifications to reduce the work function of PEDOT: PSS, this approach is not optimal for large-area fabrication.²¹ Developing scalable methods to incorporate these materials will be crucial for advancing the performance and scalability of organic photovoltaic cells.

In this study, we simulate the performance of an organic solar cell device structure with ITO/PEDOT: PSS2/DPPEZnP-TBO2/ ZnO /PEDOT: PSS1/DPPEZnP-TBO1/Al layers at 300 K. The performance of the device is analysed using the Fluxim-SETFOS simulation software. We also study the open-circuit voltage (V_{oc}), short-circuit current density (J_{sc}), fill factor (FF), and power conversion efficiency (PCE) of OSCs to show how the electrode's work function affects their performance.

Table 1: Comparison of PEDOT: PSS-based electrode solar cell devices with corresponding fill factor (FF) and power conversion efficiency (PCE)

Sl. No.	Tandem Organic Solar Cells	Fill Factor (FF)	PCE (%)	Ref.
1	ITO/PEDOT: PSS/MDMO-PPV: PCBM/ ITO/PEDOT: PSS/MDMO-PPV: PCBM/Al	56	3.1	9
2	ITO/PEDOT: PSS/MEH-PPV: PCBM/Au/ ITO/PEDOT: PSS/ MEH-PPV: PCBM/Al	45	2.4	10
3	ITO/PEDOT: PSS/ MDMO-PPV: PCBM/ZnO/PEDOT / P3HT: PCBM/Al	40	-	11
4	ITO/PEDOT: PSS/ PCPDTBT: PCBM/TiO ₂ /PEDOT/ P3HT:PC ₇₀ BM/TiO ₂ /Al	66	6.3	12
5	ITO/PEDOT: PSS/ DPPEZnP-TBO: PC61BM/PFN/Al	63.0±0.9	11.46 ± 0.28 (11.74)	13

Theory

In this work, we numerically model and investigate the electrical characteristics of organic solar cells using the commercially available program

SETFOS (Fluxim), with an emphasis on how work function affects fill factor (FF) and power conversion efficiency (PCE).²² SETFOS provides a comprehensive investigation of charge creation,

transport, and recombination mechanisms by simulating the electrical behaviour of solar systems using mathematical models. In organic photovoltaic cells, incident light creates excitons, which dissociate into free electrons and holes. The semiconductor continuity equations for electrons and holes, which are represented as follows,^{23,24} describe how these charges flow.

$$\frac{dn}{dt} = \frac{\bar{\nabla} \cdot \bar{J}_n}{-q} - R_{Langevin} - R_{nt} + g_{np}G_n \quad \dots(1)$$

$$\frac{dp}{dt} = \frac{\bar{\nabla} \cdot \bar{J}_p}{q} - R_{Langevin} - R_{pt} + g_{np}G_p \quad \dots(2)$$

In these equations, $\bar{\nabla} \cdot \bar{J}_n$ is the divergence of electron current density, $\bar{\nabla} \cdot \bar{J}_p$ is the divergence of hole current density, n corresponds to the densities of electrons, and p represents the densities of holes. The Langevin recombination rate is denoted by $R_{Langevin}$, while the corresponding recombination rates are indicated by R_{nt} and R_{pt} . The final terms in equations (1) and (2) account for optical charge generation, where g_{np} corresponds to the generation efficiency. These equations describe the behaviour of charge carriers and are coupled with Poisson's equation.

$$\bar{\nabla}(\epsilon\epsilon_0\vec{E}) = q(p - n + p_t - n_t - A_{doping} + D_{doping}) \quad \dots(3)$$

Here, q is the elementary charge, ϵ is the relative permittivity, and ϵ_0 is the vacuum permittivity, p and n are the free hole and electron concentration, p_t is the trapped hole concentration, n_t is the trapped electron concentration, \vec{E} represents the electric field, and A_{doping} and D_{doping} represent the acceptor and donor doping concentrations, respectively.

The Langevin recombination model describes the bimolecular recombination process in organic semiconductors ($R_{Langevin}$), given by

$$R_{Langevin} = \eta(\mu_n + \mu_p) \frac{q}{\epsilon} (np - n_i^2) \quad \dots(4)$$

The mobilities of electrons (μ_n) and holes (μ_p), as well as the concentrations of local charge carriers dictate the Langevin recombination rate. In this case, η is the Langevin recombination process efficiency and n_i is the intrinsic carrier concentration at thermal equilibrium.

The trap rate equation, which simulates the exchange of trapped carriers with energy levels in the organic semiconductor, describes the processes of trapping and de-trapping. For example, an electron trap interacts with the Highest Occupied Molecular Orbital (HOMO) and Lowest Unoccupied Molecular Orbital (LUMO), the levels at rates R_{te} and R_{th} , respectively, facilitating the exchange of electrons or holes.²⁵

$$\frac{dn_t}{dt} = R_{te} - R_{th} \quad \dots(5)$$

This equation describes Shockley–Read–Hall (SRH) recombination, a process in which free electrons are captured by traps and then recombine with free holes.

These simulations highlight the significant impact of the electrode work function on the performance metrics of organic solar cells. The results highlight how proper energy level alignment at the electrode interfaces minimises charge extraction barriers and recombination losses, thereby enhancing the power conversion efficiency (PCE) and fill factor (FF). This emphasises the pivotal role of electrode work function engineering in optimising device performance and guiding the design of high-efficiency, scalable organic solar cells.

Material and Methods

The electrical parameters employed in our simulations for the ITO/PEDOT: PSS2/DPPEZnP-TBO2/ ZnO /PEDOT: PSS1/DPPEZnP-TBO1/ Al structure are presented in Figure 1(a). We simulated the performance of an organic solar cell with the following layer structure: ITO, PEDOT: PSS, DPPEZnP-TBO, ZnO, PEDOT: PSS, DPPEZnP-TBO, and aluminium (Al). In this configuration, ITO and PEDOT: PSS serve as the front electrode, while Al serves as the back electrode. The cell's performance was evaluated using both flexible and rigid substrates. In this tandem OSC structure, ITO/PEDOT: PSS2/DPPEZnP-TBO2/ZnO forms the front cell, while PEDOT: PSS1/DPPEZnP-TBO1/ Al constitutes the rear cell. The two sub-cells are connected through the ZnO/PEDOT: PSS1 interlayer, enabling efficient charge recombination and current matching. PEDOT: PSS layers act as charge transport and interface modification layers

with position-dependent functions. PEDOT: PSS2 (near ITO) serves as a hole transport and anode buffer layer, enhancing ITO's work function and facilitating hole extraction. PEDOT: PSS1 (between ZnO and DPPEZnP-TBO1) operates as an interfacial recombination layer in the tandem structure. It enables efficient charge recombination and ensures proper energy alignment, thereby improving device performance.

DPPEZnP-TBO2 and DPPEZnP-TBO1 are abbreviated as layer 2 and layer 1, respectively, which act as an active layer. Figure 1(b) illustrates the energy band alignment of the layers in the

organic solar cell. It includes the energy band gap values for PEDOT: PSS, DPPEZnP-TBO, and ZnO. This alignment is crucial for understanding charge transport and efficiency in the device. DPPEZnP-TBO serves as the active layer, responsible for photon absorption, charge separation, and conducting charges to the electrodes. These include crucial measurements including fill factor (FF), power conversion efficiency (PCE), open-circuit voltage (V_{oc}), and short-circuit current density (J_{sc}). Table 2 displays the material characteristics used in the simulation of tandem organic solar cell architectures.²⁶⁻²⁸

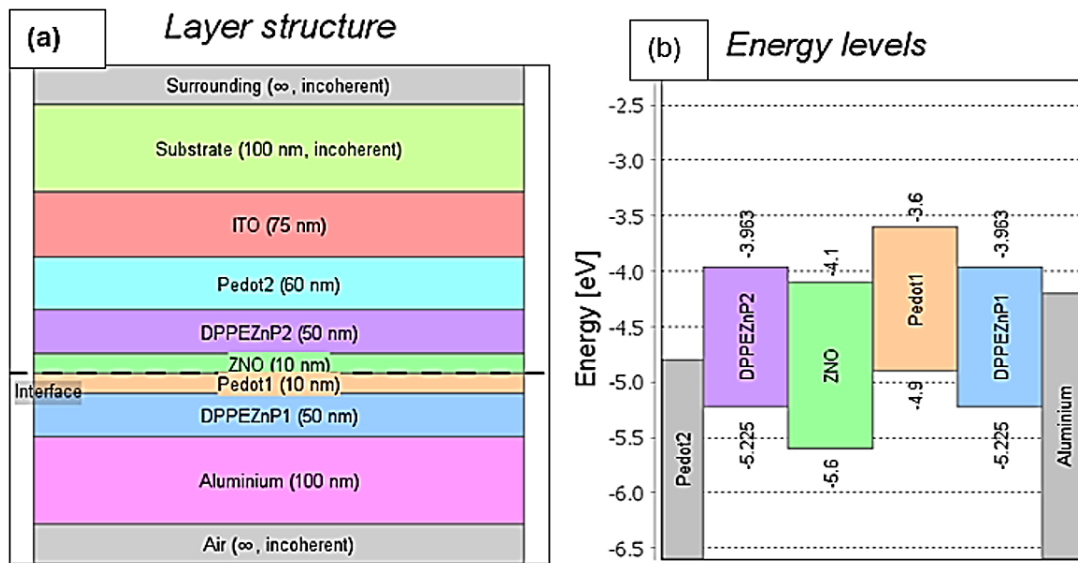


Fig.1: shows (a) the organic cell structure represented by a layer stack and (b) the energy band alignment of different layers in the OSC prior to contact.

Table 2: Simulation input parameters corresponding to the materials in tandem organic solar cell structures

Terms	DPPEZnP-TBO	ZnO	PEDOT: PSS
Bandgap	1.262	1.5	1.3
Dielectric constant	6.51	9	2.7
Mobility (μ_e)	$7.5 \times 10^{-4} \text{ cm}^2/\text{Vs}$	$100 \text{ cm}^2/\text{Vs}$	$8 \times 10^{-4} \text{ cm}^2/\text{Vs}$
Mobility (μ_p)	$3.5 \times 10^{-4} \text{ cm}^2/\text{Vs}$	$25 \text{ cm}^2/\text{Vs}$	$8 \times 10^{-4} \text{ cm}^2/\text{Vs}$
Anions (μ_e^*id)	$1 \times 10^{-10} \text{ m}^2/\text{Vs}$	$0.01 \text{ m}^2/\text{Vs}$	$1 \times 10^{-10} \text{ m}^2/\text{Vs}$
Cations (μ_p^*id)	$1 \times 10^{-10} \text{ m}^2/\text{Vs}$	$0.0025 \text{ m}^2/\text{Vs}$	$1 \times 10^{-10} \text{ m}^2/\text{Vs}$
Recombination efficiency	0.08	1	0.001
N_0	$3.713 \times 10^{27} \text{ m}^{-3}$	$1 \times 10^{26} \text{ m}^{-3}$	$1 \times 10^{26} \text{ m}^{-3}$

Results and Discussions

Charge Dynamics

Figure 2(a) presents a schematic energy level diagram illustrating the energy levels of a semiconductor in contact with electrodes. The LUMO, HOMO, electron Fermi levels, and hole Fermi levels are represented by the colours red, blue, green, and violet, respectively. It draws attention to the Fermi energy levels for electrons (E_{Fn}) and holes (E_{Fp}), as well as the Lowest Unoccupied Molecular Orbital (LUMO) and Highest Occupied Molecular Orbital (HOMO). When a semiconductor interacts with electrodes, its energy levels align relative to the electrodes' Fermi levels.²⁹ This alignment governs charge carrier (electron and hole) movement and significantly impacts the semiconductor's electrical properties, such as current conduction and junction characteristics. The diagram provides a clear visual representation of these energy levels and their interactions, offering insights into the semiconductor's behaviour with electrodes. In organic semiconductors, charge transport primarily occurs through thermally assisted tunnelling, also known as hopping, between individual molecules.³⁰ This involves thermally activated tunnelling, where thermal energy helps carriers overcome energy barriers between adjacent molecules. Figure 2(a) also demonstrates how the HOMO, LUMO, and Fermi energy levels change layer by layer. As the barrier potential between the layers decreases, the contact type transitions from non-Ohmic to Ohmic. In organic solar cells, the interface between the electrode and the active layer plays a crucial role in charge transport.³¹ Ohmic contacts are formed when the electrode's work function aligns closely with the HOMO (for hole transport) or the LUMO (for electron transport) of the organic material, enabling efficient charge flow and minimising energy loss. Conversely, non-Ohmic contacts result from significant energy barriers, which hinder charge transfer and reduce performance. Electrodes with low work functions (e.g., aluminium) are well-suited for electron transport through the LUMO. In contrast, high work function materials (e.g., gold or ITO with PEDOT: PSS) align better with the HOMO for hole transport.³² By carefully selecting electrode materials to match their work functions with the active layer's energy levels, barriers can be minimised, leading to Ohmic contacts and enhanced efficiency in organic solar cells. The colour diagram, visually shown in figure 2

(b) the variation in energy levels, highlighting distinct phases of charge transport. The colour gradients in the diagram indicate transitions between HOMO, LUMO, E_{Fn} , and E_{Fp} , emphasising the alignment or misalignment of energy levels across layers.

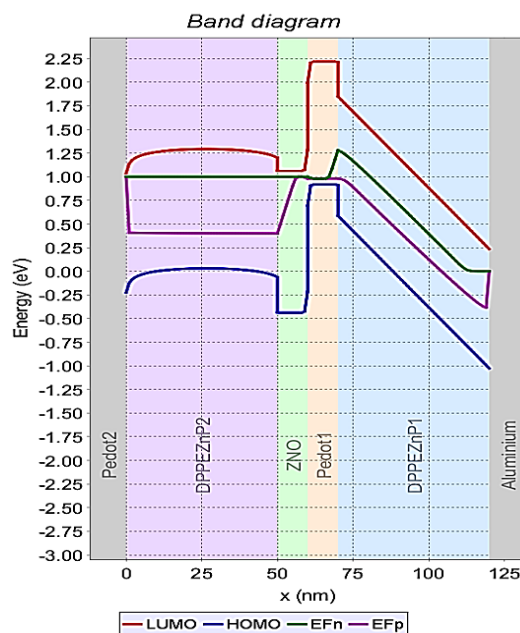


Fig.2: (a) Schematic energy level diagram of ITO/PEDOT: PSS2/DPPEZnP-TBO2/ ZnO / PEDOT: PSS1/DPPEZnP-TBO1/Al organic solar cell device structure

Figure 3 presents a layer-wise representation of (a) charge generation and (b) charge density distribution within the ITO/PEDOT: PSS2/DPPEZnP-TBO2/ ZnO /PEDOT: PSS1/DPPEZnP-TBO1/ Al solar cell structure. The ITO layer acts as the transparent conductive electrode, enabling light to pass through to the active layers without significant charge generation. PEDOT: PSS2 Layer acts as the hole transport layer, as well as improves the work function matching between the ITO electrode and the DPPEZnP-TBO2 layer. Charge generation here is minimal due to its primary role in facilitating hole extraction rather than light absorption. The DPPEZnP-TBO (DPPEZnP2) layer is the first active layer where light absorption begins. Charge generation starts increasing and remains high. The ZnO Layer acts as the electron transport layer. Charge generation in this layer is very low, as it primarily facilitates electron mobility rather than light absorption. DPPEZnP-TBO (DPPEZnP1) Layer is

the second active layer, where the significant light absorption occurs. Charge generation is moderate in this layer due to its optimised properties for absorbing photons and generating charge carriers. Charge

generation decreases linearly from the DPPEZnP1 layer towards this layer, as fewer photons remain to be absorbed. The Aluminium Layer serves as the back electrode for charge collection.

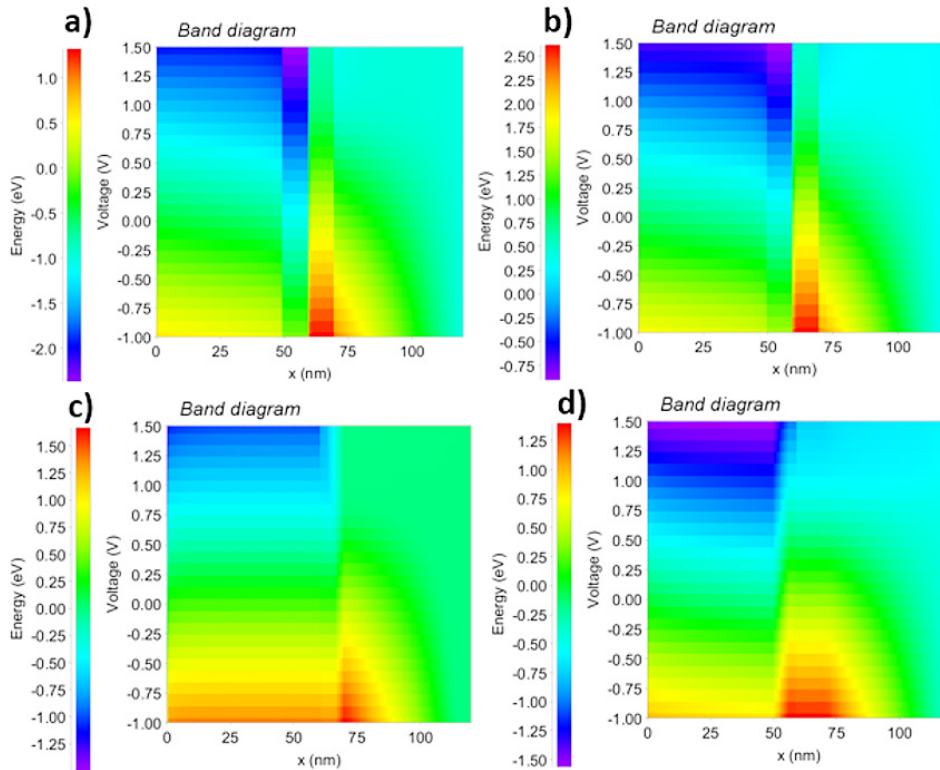


Fig.2(b): Band diagram of (a) HOMO (b) LUMO, (c) E_{FN} and (d) E_{FP}

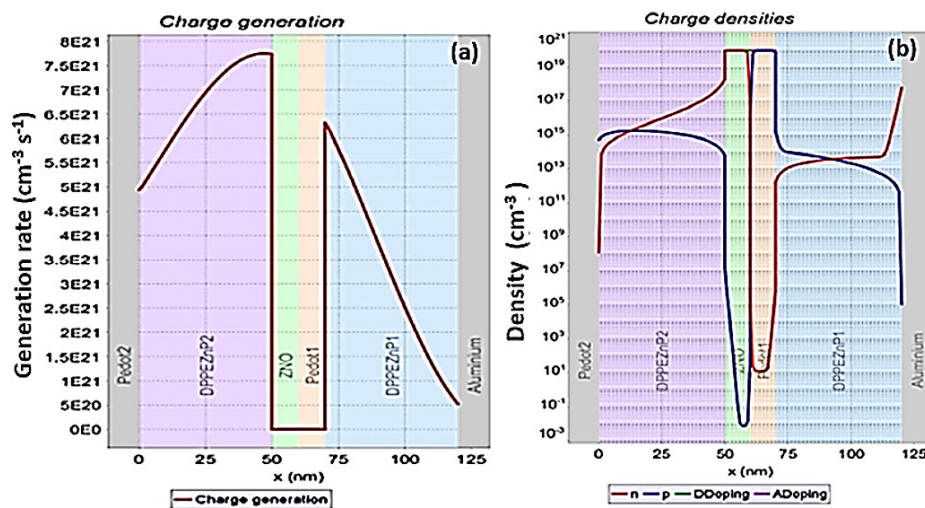


Fig.3: A representative layer-wise illustration of (a) charge generation and (b) charge density distribution in an ITO/PEDOT: PSS2/DPPEZnP-TBO2/ZnO/PEDOT: PSS1/DPPEZnP-TBO1/Al solar cell structure

In Figure 3(b), the charge density is higher in both active layers (DPPEZnP-TBO). The ZnO layer shows the highest electron density, while the PEDOT: PSS1

layer shows the highest hole density. Since the ZnO layer acts as the electron transport layer, it efficiently facilitates electron movement toward the electrode.

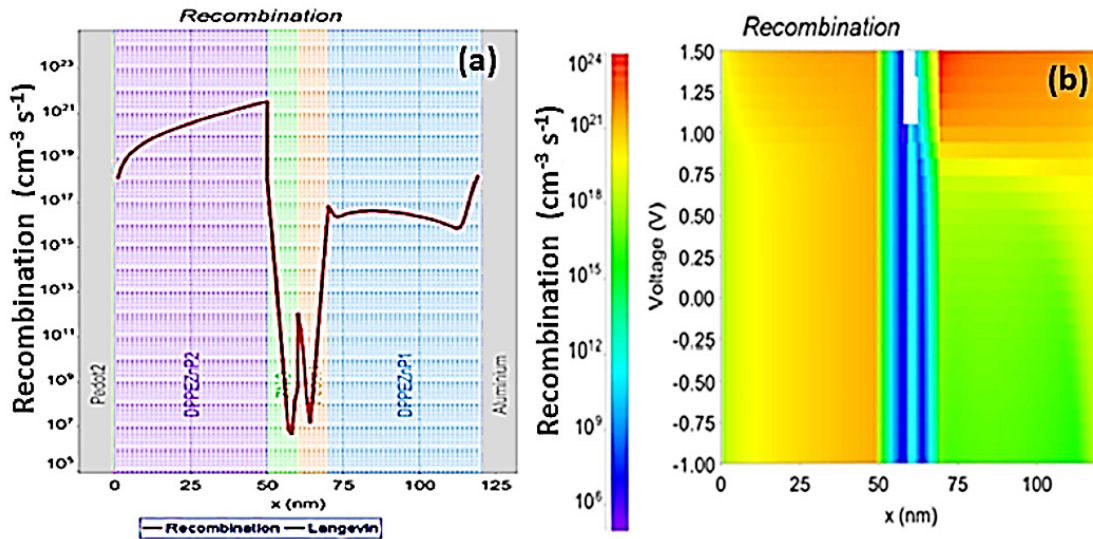


Fig.4: representative layer-wise illustration of (a) recombination and (b) layer-wise colour map of recombination in ITO/PEDOT: PSS2/DPPEZnP-TBO2/ ZnO /PEDOT: PSS1/DPPEZnP-TBO1/Al solar cell structure.

Figure 4 provides a layer-wise illustration of (a) recombination and (b) layer-wise distribution of recombination using a colour map within the ITO/PEDOT: PSS2/DPPEZnP-TBO2/ ZnO /PEDOT: PSS1/DPPEZnP-TBO1/Al solar cell, highlighting regions of charge carrier loss. These results help to identify how the layers impact device performance. The recombination rate is significantly high in the DPPEZnP-TBO layers (active layers), where most charge generation occurs, leading to greater carrier interactions. In contrast, recombination is minimal in the ZnO and PEDOT: PSS layers due to their transport-dominated roles. Figure 4(b) shows that the highest recombination occurs in the range of thickness from 0 to 50 nm and 70 to 125 nm. When PEDOT: PSS serves as the electrode, carrier recombination significantly impacts key performance metrics.

Diffusion-driven carriers may recombine before reaching the contacts, resulting in a slight reduction in the short-circuit current density (J_{SC}).³³ Under open-circuit conditions, carrier accumulation at the electrodes creates a potential difference defining the open-circuit voltage (V_{OC}).³⁴ Recombination

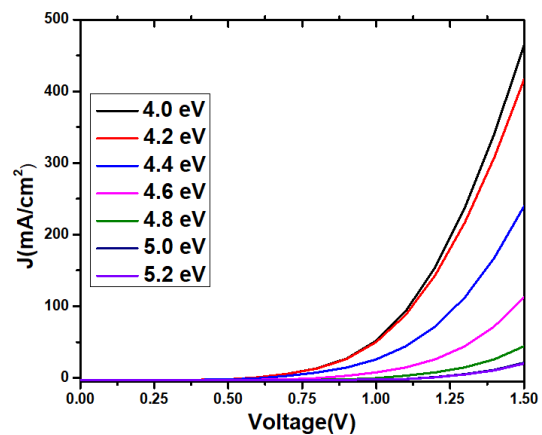


Fig.5: Current vs voltage characteristics of OSC with different work functions

narrows the separation between the electron and hole quasi-Fermi levels (E_{Fn} and E_{Fp}), lowering V_{OC} . The PEDOT: PSS work function strongly influences recombination rates and overall performance, as a stronger electric field across the absorber enhances charge separation and reduces recombination.

Current Density (J) vs Voltage (V) Analysis

Figure 5 presents the current density (J) vs voltage (V) characteristics of an ITO/PEDOT: PSS2/DPPEZnP-TBO2/ ZnO /PEDOT: PSS1/DPPEZnP-TBO1/Al organic solar cell. The J-V characteristics of organic solar cells (OSC) are strongly influenced by the work function of the electrodes because the work function determines the energy alignment between the electrodes and the organic material layers.³⁵ The work function is the energy required to move an electron from the electrode into the vacuum level, and this alignment plays a crucial role in charge injection and extraction. The work function of the electrode affects the ability of the electrode to inject charge carriers (electrons or holes) into the organic layers.³⁶ For efficient charge injection, the electrode's work function must align with the energy levels of the organic material's conduction or valence bands (LUMO for electrons, HOMO for holes). If the electrode's work function is too high or too low compared to the organic material's energy levels, a significant energy barrier forms, hindering charge injection.³⁷ After charge carriers are generated in the organic material by light absorption, they must be extracted by the electrodes. The electrode work function influences how easily charge carriers are extracted from the organic layer. If the electrode's work function is well-matched with the energy levels of the organic layer, charge extraction is efficient, and the J-V characteristics improve.

As shown in Figure 6, the open-circuit voltage (V_{oc}) increases with the PEDOT: PSS work function after it exceeds 4.2 eV, reaching a stable value of approximately 0.56 V. In contrast, the short-circuit current density (J_{sc}) follows the same trend. The J_{sc} value stabilises up to a work function of 4.4 eV, but beyond this point, it increases rapidly. In organic solar cells, the electrical properties are highly dependent on the energy level alignment between the electrode materials and the organic layers. As the PEDOT: PSS work function increases, the alignment between the electrode and the active layer improves, leading to a higher V_{oc} due to better charge separation. J_{sc} increases with increasing work function because a higher work function improves charge extraction by reducing the energy barrier at the electrode–active layer interface.³⁸

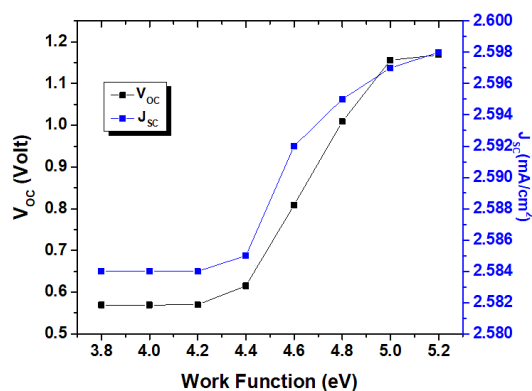


Fig.6: Open circuit voltage (V_{oc}), Short circuit current density (J_{sc}) of OSC with different work functions

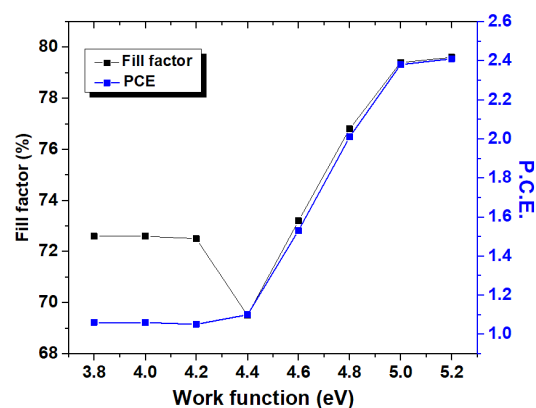


Fig.7: Fill factor (FF), Power conversion efficiency (PCE) of OSC with different work functions

Figure 7 shows that the fill Factor (FF) and power conversion efficiency (PCE) of an Organic Solar Cell (OSC) with varying anode work functions. Figure 7 shows that increasing the anode work function raises the hole density at the ITO/PEDOT: PSS interface ($x = 0$), thereby lowering the contact resistance. This inverse correlation between contact resistance and charge density at the electrode interface aligns with findings from previous studies.³⁹ Consequently, a reduction in series resistance is observed, leading to an improvement in the fill factor as the anode work function increases, thereby enhancing charge carrier extraction and overall device performance. The graph also shows the correlation between fill

factor (FF) and power conversion efficiency (PCE) of the Organic Solar Cell (OSC) at different work function values. For work functions up to 4.4 eV, both the efficiency and fill factor remain stable, indicating consistent performance. Beyond 4.4 eV, both parameters increase linearly, suggesting that higher work functions further enhance charge carrier extraction and improve the device's overall performance.

Conclusions

This study designs and analyses a planar ITO/PEDOT: PSS2/DPPEZnP-TBO2/ ZnO /PEDOT: PSS1/DPPEZnP-TBO1/Al organic solar cell using SETFOS to examine the effect of PEDOT: PSS electrode work function. Results show that optimising work function alignment between front and rear electrodes significantly impacts VOC, JSC, and FF, highlighting its crucial role in improving DPPEZnP-TBO tandem OSC performance. By varying the work function, both VOC and JSC were observed to change significantly with an increase in the work function. The best performance was achieved at a work function of 5.2 eV, resulting in a VOC of 1.16 V, JSC of 2.598 mA/cm², FF of 79.6%, and a power conversion efficiency (PCE) of 2.41%. These results suggest that optimising the electrode work function enhances charge mobility, minimises recombination losses, and improves overall device performance. This study offers key insights for enhancing the efficiency, stability, and scalability of DPPEZnP-TBO organic solar cells, supporting their potential for large-scale solar energy applications.

Acknowledgement

The authors would like to acknowledge Laxmi Narayan Dubey College, Motihari, and B.R. Ambedkar Bihar University, Muzaffarpur, for providing the simulation software, Fluxim-SETFOS.

Funding

The author(s) received no financial support for the research, authorship, and/or publication of this article

Conflict of Interest

The authors do not have any conflict of interest.

Data Availability Statement

This statement does not apply to this article.

Ethics Statement

This research did not involve human participants, animal subjects, or any material that requires ethical approval.

Informed Consent Statement

This study did not involve human participants, and therefore, informed consent was not required

Author Contributions

- **Pinaki Laha:** Writing – review and editing, Writing – original draft, Methodology, Investigation, Formal analysis, Data curation, Validation, Software.
- **Sanjay Narayan Barman:** Investigation, Formal analysis, Data curation, Validation, Software.

References

1. Nkinyam CM, Ujah CO, Nnakwo KC, Kallon DVV. Insight into organic photovoltaic cell: prospects and challenges. *Unconv Resour.* 2025;5:100121. doi:10.1016/j.unres.2024.100121
2. Ujah CO, Kallon DVV, Aikhuele DO, Aigbodion VS. Advanced composite materials: a panacea for improved electricity transmission. *Appl Sci.* 2022;12:8291. doi:10.3390/app12168291
3. Zhang MMKS, Cho HH, Yum JH. Recent advances in organic photovoltaic materials and device architectures. *Adv Energy Mater.* 2022;12:2202363. doi:10.1002/aenm.202202363
4. Riede M, Spoltore D, Leo K. Organic solar cells—The path to commercial success. *Adv Energy Mater.* 2021;11:2002653. doi:10.1002/aenm.202002653
5. Vlasov AS, Afanasev KM, Galimov AI, et al. Influence of interface states on charge transport in organic semiconductor structures. *Semiconductors.* 2024;58:187-190. doi:10.1134/S1063782624020167

6. Qasim S, Abdul Ameer F. Charge carrier recombination mechanisms in polymer-based optoelectronic devices. *Semiconductors*. 2025;59:507-512. doi:10.1134/S1063782625600342
7. Song W, Peng R, Huang L, *et al.* Over 14% efficiency folding-flexible ITO-free organic solar cells enabled by eco-friendly acid-processed electrodes. *iScience*. 2020;23:100981. doi:10.1016/j.isci.2020.100981
8. Zhao C, Tang CG, Seah ZL, *et al.* Improving organic photovoltaic cells by forcing electrode work function well beyond onset of ohmic transition. *Nat Commun*. 2021;12:2250. doi:10.1038/s41467-021-22358-y
9. Kawano K, Ito N, Nishimori T, Sakai J. High-performance bulk heterojunction organic solar cells using poly(3-hexylthiophene) and fullerene derivatives. *Appl Phys Lett*. 2006;88:073514. doi:10.1063/1.2177633
10. Shrotriya V, Wu EH, Li G, Yao Y, Yang Y. Efficient light harvesting in multiple-device stacked structure for polymer solar cells. *Appl Phys Lett*. 2006;88:064104. doi:10.1063/1.2172741
11. Gilot J, Wienk MM, Janssen RAJ. Double and triple junction polymer solar cells processed from solution. *Appl Phys Lett*. 2007;90:143512. doi:10.1063/1.2345612
12. Kim JY, Lee K, Coates NE, *et al.* Efficient tandem polymer solar cells fabricated by all-solution processing. *Science*. 2007;317:222-225. doi:10.1126/science.1141711
13. Li M, Gao K, Wan X, *et al.* Solution-processed organic tandem solar cells with power conversion efficiencies over 12%. *Nat Photonics*. 2017;11:85-90. doi:10.1038/nphoton.2016.240
14. Fan X, Stott NE, Zeng J, *et al.* Efficient and stable organic solar cells enabled by interfacial energy level modulation. *J Mater Chem A*. 2023;11:18561-18570. doi:10.1039/D3TA03213B
15. Hu L, Song J, Yin X, Su Z, Li Z. Research progress on polymer solar cells based on PEDOT: PSS electrodes. *Polymers*. 2020;12:145. doi:10.3390/polym12010145
16. Yu Z, Xia Y, Du D, Ouyang J. PEDOT: PSS films with enhanced conductivity via post-treatment for flexible electronics. *ACS Appl Mater Interfaces*. 2016;8:11629-11638. doi:10.1021/acsami.6b00317
17. Li Z, Liang Y, Zhong Z, *et al.* Highly conductive and transparent PEDOT: PSS films for optoelectronic applications. *Synth Met*. 2015;210:363-370. doi:10.1016/j.synthmet.2015.11.006
18. Zhou Y, Cheun H, Choi S, Fuentes-Hernandez C, Kippelen B. Indium tin oxide-free and metal-free semitransparent organic solar cells. *Science*. 2011;332:316-319. doi:10.1126/science.1218829
19. Ouyang J. Solution-processed PEDOT:PSS films with conductivity enhancement for organic electronics. *Displays*. 2013;34:5-9. doi:10.1016/j.displa.2013.08.007
20. Chang YM, Wang L, Su WF. Improving the efficiency of polymer solar cells using modified buffer layers. *Org Electron*. 2008;9:968-973. doi:10.1016/j.orgel.2008.07.003
21. Li Z, Qin F, Liu T, *et al.* Interface engineering for high-performance inverted polymer solar cells. *Org Electron*. 2015;21:1-8. doi:10.1016/j.orgel.2015.01.012
22. FluximAG. SETFOS, version 5.5. Switzerland; 2023. Accessed 2023. <https://www.fluxim.com>
23. Feron K, Belcher WJ, Fell CJ, Dastoor PC. Organic solar cells: understanding the role of interlayers. *Int J Mol Sci*. 2012;13:17019-17047. doi:10.3390/ijms131217019
24. Salem MS, Shaker A, Abouelatta M, Saeed A. Performance enhancement of organic solar cells using interface engineering. *Polymers*. 2023;15:784. doi:10.3390/polym15030784
25. Neukom M. *Comprehensive Characterisation and Modelling of Operation Mechanisms in Third Generation Solar Cells*. Augsburg, Germany: University of Augsburg; 2019.
26. Li XD, Chen TP, Liu P, Liu Y, Liu Z, Leong KC. Electrical characterization of organic semiconductor devices using impedance spectroscopy. *J Appl Phys*. 2014;115:1-6. doi:10.1063/1.4868338
27. Jan H, Mathew S, Bhotla PV. Interface-dependent charge transport in organic electronic devices. *ACS Appl Electron Mater*. 2024. doi:10.1021/acsaelm.4c01098
28. Rawat M, Laha P. Charge transport modeling in organic thin-film devices. *Bull Mater Sci*. 2025;48:112. doi:10.1007/s12034-025-03466-7

29. Gobbi M, Pietrobon L, Atxabal A, *et al.* Charge injection and transport in organic semiconductors probed by magnetoresistance. *Nat Commun.* 2014;5:4161. doi:10.1038/ncomms5161
30. Coropceanu V, Cornil J, da Silva Filho DA, Olivier Y, Silbey R, Brédas JL. Charge transport in organic semiconductors. *Chem Rev.* 2007;107:926-952. doi:10.1021/cr050140x
31. Rahimi R, Roberts A, Narang V, Kumbham VK, Korakakis D. Optical modeling of multilayer organic optoelectronic devices. *Opt Mater.* 2013;35:5-11. doi:10.1016/j.optmat.2012.12.011
32. Yi C, Hu X, Gong X, Elzatahry A. Interface and morphology control in organic optoelectronics. *Mater Today.* 2016;19:3-10. doi:10.1016/j.mattod.2015.11.003
33. Sherkar TS, Momblona C, Gil-Escrig L, *et al.* Recombination mechanisms in perovskite and organic solar cells. *ACS Energy Lett.* 2017;2:1214-1222. doi:10.1021/acsenerylett.7b00236
34. Li C, Lv L, Qin L, *et al.* Influence of interfacial layers on organic photovoltaic performance. *Materials.* 2018;11:2407. doi:10.3390/ma11122407
35. Khalf A, Gojanovic J, Cirovic N, Zivanovic S, Matavulj P. Numerical modeling of organic solar cell devices. *IEEE J Photovolt.* 2020;10:1-8. doi:10.1109/JPHOTOV.2020.2965401
36. Lee H, Cho SW, Park SH, Cho MH, Yi Y. Interface engineering in organic optoelectronic devices. *Mater Res Bull.* 2014;58:19-23. doi:10.1016/j.materresbull.2014.05.010
37. Lee JH, Kim JJ. Charge injection and transport in organic light-emitting devices. *Phys Status Solidi A.* 2012;209:8-14. doi:10.1002/pssa.201228199
38. Shuttle CG, Hamilton R, O'Regan BC, Nelson J, Durrant JR. Charge-density dependence of open-circuit voltage in organic solar cells. *Proc Natl Acad Sci U S A.* 2010;107:16448-16452. doi:10.1073/pnas.1004363107
39. Tan JK, Png RQ, Zhao C, *et al.* Trap-assisted recombination in organic semiconductor devices. *Nat Commun.* 2018;9:3269. doi:10.1038/s41467-018-05200-w